Analysis of experimental error sources in a linear-optics quantum gate

2010 New J. Phys. 12 043053

(http://iopscience.iop.org/1367-2630/12/4/043053)

New Journal of Physics
The open-access journal for physics

Analysis of experimental error sources in a linear-optics quantum gate

T Nagata[1,2], R Okamoto[1,2], H F Hofmann[3] and S Takeuchi[1,2,4]

[1] Research Institute for Electronic Science, Hokkaido University, Sapporo 001-0020, Japan

[2] The Institute of Scientific and Industrial Research, Osaka University, Ibaraki, Osaka 567-0047, Japan

[3] Graduate School of Advanced Sciences of Matter, Hiroshima University, Higashi-Hiroshima 739-8530, Japan

E-mail: takeuchi@es.hokudai.ac.jp

New Journal of Physics **12** (2010) 043053 (17pp)
Received 27 November 2009
Published 30 April 2010
Online at http://www.njp.org/
doi:10.1088/1367-2630/12/4/043053

Abstract. Possible error sources in an experimentally realized linear-optics controlled-Z gate (Okamoto *et al* 2005 *Phys. Rev. Lett.* **95** 210506) are analyzed by considering the deviations of the beam splitting ratios from the ideal values (δR_{H}, δR_{V}), the polarization-dependent phase shift (birefringence) of the optical components ($\delta\phi$) and the mode mismatch of input photons ($\delta\xi$). It is found that the error rate is linearly dependent on δR_{V} and $\delta\xi$, while the dependence on δR_{H} and $\delta\phi$ is approximately quadratic. As a practical result, the gate is much more sensitive to small errors in R_{V} than in R_{H}. Specifically, the reflectivity error for vertical polarization must be less than 0.1% to realize a gate with an error of less than 0.1%, whereas the reflectivity error for horizontal polarization can be up to 1%. It is also shown that the effects of different error sources are not independent of each other (linear error model). Under certain conditions, the deviation from the linear error model exceeds 10% of the total error. The method of analysis used illustrates the basic features of errors in general linear optics quantum gates and circuits, and can easily be adapted to any other device of this type.

[4] Author to whom any correspondence should be addressed.

Contents

1. Introduction

Quantum information science enables us to improve the performance of certain tasks by exploiting quantum mechanical effects. Photons have been widely used for quantum communication [1], quantum metrology [2, 3] and quantum lithography [4, 5]. Using the dual-rail scheme [6], qubits can be encoded in one photon in two modes, e.g. the polarization degrees of freedom. The main advantages of photonic qubits are their robustness against decoherence and their suitability for single-qubit operations. However, two-qubit gates require strong interaction between single photons, which may necessitate extremely high optical nonlinearity. In 2001, Knill *et al* discovered a way to overcome this problem by proposing a controlled-Z (CZ) gate where the correct gate operation is heralded by a success signal, resulting in a possible implementation of scalable quantum computation where only the heralded operations are selected [7]. This method uses linear optics, photon-number-resolving detectors [8, 9] and single-photon sources [10]. Motivated by this discovery, a closely related proposal of a post-selected CZ gate, where the successful gate operation is identified by post-selecting the correct photon distribution in the output modes, was introduced [11, 12] and eventually realized by a very compact optical circuit using partially polarizing beam splitters (PPBSs) [13]–[15]. Similar linear optics quantum circuits have also been demonstrated, both for heralded [16] and post-selected [17, 18] schemes.

In such quantum circuits, errors in one gate generally propagate to the next gate and thus the errors tend to accumulate. Consequently, it is critical to analyze the errors in each gate to achieve high-fidelity operation for quantum circuits. In an early study, Ralph *et al* [12] analyzed the output states of the linear-optics CZ gate for a typical set of input states. They considered two error sources, incorrect beam-splitting ratios and spatio-temporal mode mismatching at the two-photon interference, and calculated the fidelity of the output states to the ideal ones (Bell states). Kiesel *et al* [15] derived a full process matrix of a linear-optics CZ gate taking the gate

errors into account. Recently, Weinhold *et al* [19] considered the impact of errors observed in reconstructed process matrices on the fault tolerance of quantum computation. In particular, they pointed out the importance of controlling the photon numbers in the input modes.

In this paper, we consider the joint effect of errors in the optical elements and mode matching in the multi-photon interference by analyzing the dependence of the quantum coherent operation in the Hilbert space of photon polarization on the experimental parameters. Specifically, we include errors in the reflectivities and a possible polarization-dependent phase shift (birefringence), which has not been considered in the previous analysis [12, 15, 19] of the beam splitter. Another important source of errors may be the combination of excess input photons and photon loss [19]. However, this error mainly depends on the type of photon source used. Since this paper focuses on errors in the operation of the device itself, we chose not to include such errors.

We show that the effects of the reflectivity error in the vertical polarization are far more significant than the effects of errors in the horizontal polarization or the birefringence. We also investigate how the various causes of errors interact with each other. One of the problems in the comparison of different error sources is the fact that the errors are not independent of each other, so that a linear error model where the total error is given by a simple sum of all errors is not valid. We evaluate the extent to which the errors are influenced by the presence of other error sources and show that the deviation from the linear error model can exceed 10% of the total error under certain conditions. Furthermore, we discuss the requirements for achieving a small total error (e.g. 0.001), for future scalable optical quantum computations [20].

This paper is organized as follows. In section 2, we describe the method used to analyze the gate and the causes of errors included in our model. First, we briefly introduce a PPBS-based CZ gate and derive the operator describing the gate operation in the post-selected Hilbert space of two-photon polarization. Then, we introduce the experimental error sources and describe the modified gate operation in the post-selected Hilbert space. Finally, we show how the process fidelity and the associated error rate can be derived from this formulation of the imperfect gate operation. In section 3, we present and discuss the results of the analysis. We show how each error source contributes to the total error rate and identify the mutual dependence of error sources in terms of the deviation from the linear error model. Finally, the conditions for achieving a low error rate are discussed. Section 4 concludes the paper.

2. Cause of errors and the error analysis method

2.1. A compact CZ gate using PPBSs

The construction of CZ gates using PPBSs was reported in 2005 [13]–[15]. In this scheme, the separate path interferences of the original theoretical proposal [11, 12] are replaced with a single polarization-dependent interference at a PPBS, making the gates more compact and robust against vibrations. Figure 1 shows a schematic diagram of the CZ gate. Two photons in modes C_{in} and T_{in} generated by single photon sources are simultaneously input to PPBS-A. The reflectivities of PPBS-A are 1/3 for horizontally polarized light and 1 for vertically polarized light. These reflectivities therefore generate two-photon quantum interference [21] for only the horizontally polarized photons. At the gate output, we select the cases in which single photons are emitted to both output modes, C_{out} and T_{out}. This combination of two-photon interference and post-selection flips the phase of the input state only when both of the input photons

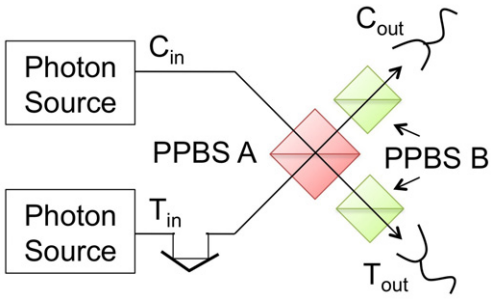

Figure 1. A schematic diagram of the compact linear-optics CZ gate.

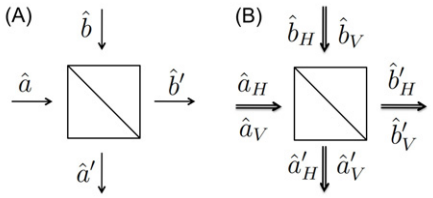

Figure 2. Operators of input and output modes for (A) beam splitter and (B) PPBS.

are horizontally polarized. However, the operation also attenuates the probability amplitude of horizontally polarized photons while preserving that of vertically polarized photons. To compensate for this difference in the probability amplitudes of horizontally and vertically polarized photons, two PPBS-Bs are inserted at both output modes of PPBS-A. The gate then functions as a CZ gate for horizontal and vertical basis with a success probability of 1/9.

As described above, PPBS-A is the key component, while PPBS-B is a supplemental component. Indeed, the errors caused by PPBS-Bs can be easily compensated since the PPBS-B acts only on single-qubit inputs. Consequently, we consider only the errors caused by PPBS-A in the following analysis.

2.2. A unitary operator for a PPBS

A beam splitter is an optical element that has two spatial modes each as its input (a, b) and output (a′, b′). We use the annihilation operators $\hat{a}$, $\hat{b}$, $\hat{a}$ and $\hat{b}$ for photons in the corresponding modes (figure 2(A)). When there are no losses at the beam splitter, the relationship between the operators can be expressed using the following matrix representation for the beam splitter [22]:

$$\begin{pmatrix} \hat{a}' \\ \hat{b}' \end{pmatrix} = \mathbf{U}_{\mathrm{BS}} \begin{pmatrix} \hat{a} \\ \hat{b} \end{pmatrix} = \begin{pmatrix} \sqrt{R} & \mathrm{i}\sqrt{1-R} \\ \mathrm{i}\sqrt{1-R} & \sqrt{R} \end{pmatrix} \begin{pmatrix} \hat{a} \\ \hat{b} \end{pmatrix}, \tag{1}$$

where R is the reflectivity of the beam splitter.

In contrast, a PPBS has four modes for input and output by including the polarization degree of freedom. We use the annihilation operators $\hat{a}_{\mathrm{H}}$, $\hat{b}_{\mathrm{H}}$, $\hat{a}_{\mathrm{V}}$, $\hat{b}_{\mathrm{V}}$, $\hat{a}'_{\mathrm{H}}$, $\hat{b}'_{\mathrm{H}}$, $\hat{a}'_{\mathrm{V}}$ and $\hat{b}'_{\mathrm{V}}$ for the corresponding modes (figure 2(B)). A horizontally (vertically) polarized photon at the input

preserves its polarization at the output, but the reflectivities are different for the two orthogonal polarizations. The relationship between input and output operators can then be expressed as

$$\begin{pmatrix} \hat{a}'_{\mathrm{H}} \\ \hat{b}'_{\mathrm{H}} \\ \hat{a}'_{\mathrm{V}} \\ \hat{b}'_{\mathrm{V}} \end{pmatrix} = \mathbf{U}_{\mathrm{PPBS}} \begin{pmatrix} \hat{a}_{\mathrm{H}} \\ \hat{b}_{\mathrm{H}} \\ \hat{a}_{\mathrm{V}} \\ \hat{b}_{\mathrm{V}} \end{pmatrix}, \tag{2}$$

$$\begin{aligned} \mathbf{U}_{\mathrm{PPBS}} &= \begin{pmatrix} \mathbf{U}_{\mathrm{BSH}} & 0 \\ 0 & \mathrm{e}^{\mathrm{i}\phi}\mathbf{U}_{\mathrm{BSV}} \end{pmatrix} \\ &= \begin{pmatrix} \sqrt{R_{\mathrm{H}}} & \mathrm{i}\sqrt{1-R_{\mathrm{H}}} & 0 & 0 \\ \mathrm{i}\sqrt{1-R_{\mathrm{H}}} & \sqrt{R_{\mathrm{H}}} & 0 & 0 \\ 0 & 0 & \mathrm{e}^{\mathrm{i}\phi}\sqrt{R_{\mathrm{V}}} & \mathrm{i}\mathrm{e}^{\mathrm{i}\phi}\sqrt{1-R_{\mathrm{V}}} \\ 0 & 0 & \mathrm{i}\mathrm{e}^{\mathrm{i}\phi}\sqrt{1-R_{\mathrm{V}}} & \mathrm{e}^{\mathrm{i}\phi}\sqrt{R_{\mathrm{V}}} \end{pmatrix}, \end{aligned} \tag{3}$$

where ϕ is the phase difference between horizontally polarized light and vertically polarized light and R_{H} and R_{V} are the reflectivities of horizontally and vertically polarized light, respectively.

2.3. *Operation formalisms for an ideal CZ gate*

In the ideal case, the parameters of PPBS-A are $R_{\mathrm{H}} = 1/3$, $R_{\mathrm{V}} = 1$ and $\phi = 0$, so that the matrix for PPBS-A can be expressed as

$$\mathbf{U}_{\mathrm{PPBSA}} = \begin{pmatrix} \sqrt{1/3} & \mathrm{i}\sqrt{2/3} & 0 & 0 \\ \mathrm{i}\sqrt{2/3} & \sqrt{1/3} & 0 & 0 \\ 0 & 0 & 1 & 0 \\ 0 & 0 & 0 & 1 \end{pmatrix}. \tag{4}$$

When the input state of PPBS-A is $|H, H\rangle_{\mathrm{a,b}} = \hat{a}^{\dagger}_{\mathrm{H}}\hat{b}^{\dagger}_{\mathrm{H}}|0\rangle$ corresponding to two horizontally polarized photons input from opposite signs, the output state can be derived using the transformation of the creation operators defined by equations (2) and (4) as follows:

$$\begin{aligned} \mathbf{U}_{\mathrm{PPBSA}}\hat{a}^{\dagger}_{\mathrm{H}}\hat{b}^{\dagger}_{\mathrm{H}}|0\rangle &= \left(\frac{1}{\sqrt{3}}\hat{a}'_{\mathrm{H}} + \mathrm{i}\frac{\sqrt{2}}{\sqrt{3}}\hat{b}'_{\mathrm{H}}\right)^{\dagger}\left(\mathrm{i}\frac{\sqrt{2}}{\sqrt{3}}\hat{a}'_{\mathrm{H}} + \frac{1}{\sqrt{3}}\hat{b}'_{\mathrm{H}}\right)^{\dagger}|0\rangle \\ &= \left(-\frac{1}{3}\hat{a}'_{\mathrm{H}}\hat{b}'_{\mathrm{H}} + \mathrm{i}\frac{\sqrt{2}}{3}\hat{a}'^{2}_{\mathrm{H}} + \mathrm{i}\frac{\sqrt{2}}{3}\hat{b}'^{2}_{\mathrm{H}}\right)^{\dagger}|0\rangle \\ &= -\frac{1}{3}|\mathrm{H}, \mathrm{H}\rangle_{\mathrm{a}',\mathrm{b}'} - \mathrm{i}\frac{2}{3}|2\mathrm{H}, 0\rangle_{\mathrm{a}',\mathrm{b}'} - \mathrm{i}\frac{2}{3}|0, 2\mathrm{H}\rangle_{\mathrm{a}',\mathrm{b}'}. \end{aligned} \tag{5}$$

The complete transformation for an arbitrary state can be obtained by applying the transformation $\mathbf{U}_{\mathrm{PPBSA}}$ to the creation operators of the remaining three basis states,

$$\mathbf{U}_{\mathrm{PPBS\,A}}|\mathrm{H}, \mathrm{V}\rangle_{\mathrm{a,b}} = \frac{1}{\sqrt{3}}|\mathrm{H}, \mathrm{V}\rangle_{\mathrm{a}',\mathrm{b}'} - \mathrm{i}\sqrt{\frac{2}{3}}|0, \mathrm{VH}\rangle_{\mathrm{a}',\mathrm{b}'}, \tag{6}$$

$$\mathbf{U}_{\mathrm{PPBS\,A}}\,|\mathrm{V},\mathrm{H}\rangle_{\mathrm{a,b}} = \frac{1}{\sqrt{3}}\,|\mathrm{V},\mathrm{H}\rangle_{\mathrm{a',b'}} - \mathrm{i}\sqrt{\frac{2}{3}}\,|\mathrm{VH},0\rangle_{\mathrm{a',b'}}, \tag{7}$$

$$\mathbf{U}_{\mathrm{PPBS\,A}}\,|\mathrm{V},\mathrm{V}\rangle_{\mathrm{a,b}} = |\mathrm{V},\mathrm{V}\rangle_{\mathrm{a',b'}}. \tag{8}$$

For the CZ operation, we post-select the cases where single photons are in both output modes, a′ and b′. With ideal PPBS-Bs ($R_{\mathrm{H}} = 0$, $R_{\mathrm{V}} = 2/3$) in the output modes of the PPBS, the output state of our CZ gate will be

$$\begin{aligned}
\hat{L}\,|\mathrm{H},\mathrm{H}\rangle_{\mathrm{C_{in},T_{in}}} &= -\tfrac{1}{3}\,|\mathrm{H},\mathrm{H}\rangle_{\mathrm{C_{out},T_{out}}},\\
\hat{L}\,|\mathrm{H},\mathrm{V}\rangle_{\mathrm{C_{in},T_{in}}} &= \tfrac{1}{3}\,|\mathrm{H},\mathrm{V}\rangle_{\mathrm{C_{out},T_{out}}},\\
\hat{L}\,|\mathrm{V},\mathrm{H}\rangle_{\mathrm{C_{in},T_{in}}} &= \tfrac{1}{3}\,|\mathrm{V},\mathrm{H}\rangle_{\mathrm{C_{out},T_{out}}},\\
\hat{L}\,|\mathrm{V},\mathrm{V}\rangle_{\mathrm{C_{in},T_{in}}} &= \tfrac{1}{3}\,|\mathrm{V},\mathrm{V}\rangle_{\mathrm{C_{out},T_{out}}},
\end{aligned} \tag{9}$$

where $\hat{L} = 1/3\hat{U}_{\mathrm{CZ}}$ describes the ideal gate process including the post-selection with $\hat{U}_{\mathrm{CZ}} = -|\mathrm{H},\mathrm{H}\rangle\langle\mathrm{H},\mathrm{H}| + |\mathrm{H},\mathrm{V}\rangle\langle\mathrm{H},\mathrm{V}| + |\mathrm{V},\mathrm{H}\rangle\langle\mathrm{V},\mathrm{H}| + |\mathrm{V},\mathrm{V}\rangle\langle\mathrm{V},\mathrm{V}|$. This operation is essentially a CZ gate $\hat{U}_{\mathrm{CZ}}$ with a success probability of 1/9. By using the logical basis states $|\bar{0}\rangle_{\mathrm{T}} \equiv (|\mathrm{V}\rangle_{\mathrm{T}} + |\mathrm{H}\rangle_{\mathrm{T}})$ and $|\bar{1}\rangle_{\mathrm{T}} \equiv (|\mathrm{V}\rangle_{\mathrm{T}} - |\mathrm{H}\rangle_{\mathrm{T}})$ for the target qubit and $|\bar{0}\rangle_{\mathrm{C}} \equiv |\mathrm{V}\rangle_{\mathrm{C}}$ and $|\bar{1}\rangle_{\mathrm{C}} \equiv |\mathrm{H}\rangle_{\mathrm{C}}$ for the control qubit, this operation corresponds to a controlled-NOT gate.

2.4. Operation formalism for a CZ gate including error sources

In this paper, we consider the birefringence error and the non-ideal reflectivities introduced by imperfections in PPBS-A, along with the spatio-temporal mode mismatch at the two-photon interference. When using parametric down-conversion, another important source of errors may be the combination of excess input photons and photon loss [19]. However, this error mainly depends on the type of photon source used. Since this paper focuses on errors in the operation of the device itself, we chose not to include such errors.

2.4.1. Birefringence and non-ideal reflectivities of the PPBS. Equation (3) shows how errors in the reflectivity and the phase shift between horizontal and vertical polarizations can be included in the operation of the gate. In the following, δR_{H} and δR_{V} will be used to describe the deviations of the reflectivities R'_{H} and R'_{V} from the ideal reflectivities (i.e. the reflectance errors):

$$\delta R_{\mathrm{H}} = R_{\mathrm{H}}{}' - 1/3, \tag{10}$$

$$\delta R_{\mathrm{V}} = 1 - R_{\mathrm{V}}{}'. \tag{11}$$

Likewise, ϕ in equation (3) becomes an error source (birefringence error). Here the 'birefringence error' originates from a polarization-dependent optical phase that is unintentionally added when light is reflected by the PPBS. We define the birefringence error as the deviation of ϕ' from its ideal value of zero,

$$\delta\phi = \phi'. \tag{12}$$

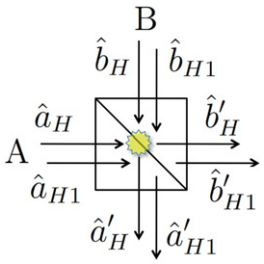

Figure 3. Schematic diagram of operators for PPBS-A that include the effects of mode mismatch. (Operators of vertically polarized photons are not shown.) Ancillary mode $\hat{a}_{\mathrm{H1}}$ ($\hat{a}_{\mathrm{V1}}$) does not interfere with $\hat{b}_{\mathrm{H}}$ ($\hat{b}_{\mathrm{V}}$) at all, while $\hat{a}_{\mathrm{H}}$ ($\hat{a}_{\mathrm{V}}$) interferes with $\hat{b}_{\mathrm{H}}$ ($\hat{b}_{\mathrm{V}}$) perfectly. Note that the figure is a schematic diagram and the ancillary spatio-temporal mode $\hat{a}_{\mathrm{H1}}$ ($\hat{a}_{\mathrm{V1}}$) does not always propagate in parallel to $\hat{a}_{\mathrm{H}}$ ($\hat{a}_{\mathrm{V}}$).

2.4.2. Spatio-temporal mode mismatch. For the ideal operation, equation (9) was derived by assuming that the input photons are in single modes and are perfectly mode-matched (i.e. they are indistinguishable) at PPBS-A. In practice, however, the modes of these photons are partially mismatched in space and time or frequency due to factors such as misalignment or intrinsic jitter of the single-photon arrival time. These types of errors can be analyzed using ancillary modes ($\hat{a}_{\mathrm{H1}}$, $\hat{b}_{\mathrm{H1}}$, $\hat{a}_{\mathrm{V1}}$, $\hat{b}_{\mathrm{V1}}$) (figure 3) and the mode-matching parameter ξ. Here, we define new operators for input port A to include the effect of the mode mismatch as

$$\hat{a}_{\mathrm{H0}} = \sqrt{\xi}\hat{a}_{\mathrm{H}} + \sqrt{1-\xi}\hat{a}_{\mathrm{H1}}, \tag{13}$$

$$\hat{a}_{\mathrm{V0}} = \sqrt{\xi}\hat{a}_{\mathrm{V}} + \sqrt{1-\xi}\hat{a}_{\mathrm{V1}}, \tag{14}$$

where $\hat{a}_{\mathrm{H}}$ ($\hat{a}_{\mathrm{V}}$) interferes with $\hat{b}_{\mathrm{H}}$ ($\hat{b}_{\mathrm{V}}$) perfectly, while $\hat{a}_{\mathrm{H1}}$ ($\hat{a}_{\mathrm{V1}}$) does not interfere with $\hat{b}_{\mathrm{H}}$ ($\hat{b}_{\mathrm{V}}$) at all. In the following, the photon in input port A is considered to be a superposition of these two modes ($\hat{a}_{\mathrm{H0}}$ ($\hat{a}_{\mathrm{V0}}$)), while the photon in input port B is in mode $\hat{b}_{\mathrm{H}}$ ($\hat{b}_{\mathrm{V}}$). Note that the use of a mixture of operators instead of a superposition in equations (13) and (14) results in the same result. The parameter ξ is equivalent to the visibility of the two-photon Hong–Ou–Mandel interference at a 50/50 beam splitter (appendix). Just as for the other error sources, we define the deviation of $\delta\xi$ from the ideal value of 1 as

$$\delta\xi = 1 - \xi. \tag{15}$$

Since the modes $\hat{a}_{\mathrm{H}}$ and $\hat{a}_{\mathrm{H1}}$ are orthogonal, the output modes of $\hat{a}_{\mathrm{H}}$ and $\hat{a}_{\mathrm{H1}}$ are also orthogonal. We can therefore assume that the ancillary modes form an additional set of modes transformed by the PPBS-A according to

$$\begin{pmatrix} \hat{a}'_{\mathrm{H1}} \\ \hat{b}'_{\mathrm{H1}} \\ \hat{a}'_{\mathrm{V1}} \\ \hat{b}'_{\mathrm{V1}} \end{pmatrix} = \mathbf{U}_{\mathrm{PPBS}} \begin{pmatrix} \hat{a}_{\mathrm{H1}} \\ \hat{b}_{\mathrm{H1}} \\ \hat{a}_{\mathrm{V1}} \\ \hat{b}_{\mathrm{V1}} \end{pmatrix}, \tag{16}$$

where $\hat{a}'_{\mathrm{H1}}$, $\hat{b}'_{\mathrm{H1}}$ ($\hat{a}'_{\mathrm{V1}}$ and $\hat{b}'_{\mathrm{V1}}$) are the output modes shown in figure 3.

2.5. Process operators and process fidelity

To analyze the process fidelity in the presence of errors, we need a complete description of the post-selected gate process with errors such as the one given in equation (9). To obtain such a description, we follow a procedure similar to that given by equations (5)–(8), substituting the modified values of R_{H}, R_{V} and ϕ. To include the mode matching effect, we first consider a complete mode mismatch. In that case, photons in the input modes $\hat{a}_i$ are distinguishable from photons in the input modes $\hat{b}_i$, and the reflection process of both photons at the PPBS does not interfere with the transmission process of both photons. Therefore, the effects of reflection and transmission processes on the polarization state of the two photons can be described by two separate operators, $\hat{S}_{\mathrm{R}}$ and $\hat{S}_{\mathrm{T}}$. Assuming that the additional PPBS-Bs in the output are ideal ($R_{\mathrm{H}} = 0$, $R_{\mathrm{V}} = 2/3$),

$$\hat{S}_{\mathrm{R}} = \left(\frac{1}{3} + \delta R_{\mathrm{H}}\right) |\mathrm{H},\mathrm{H}\rangle\langle \mathrm{H},\mathrm{H}| + \frac{1}{\sqrt{3}} \mathrm{e}^{\mathrm{i}\phi} \sqrt{(1-\delta R_{\mathrm{V}})\left(\frac{1}{3} + \delta R_{\mathrm{H}}\right)} (|\mathrm{H},\mathrm{V}\rangle\langle \mathrm{H},\mathrm{V}| + |\mathrm{V},\mathrm{H}\rangle\langle \mathrm{V},\mathrm{H}|) + \frac{1}{3} \mathrm{e}^{\mathrm{i}2\phi} (1 - \delta R_{\mathrm{V}})\, |\mathrm{V},\mathrm{V}\rangle\langle \mathrm{V},\mathrm{V}|, \tag{17}$$

$$\hat{S}_{\mathrm{T}} = -\left(\frac{2}{3} - \delta R_{\mathrm{H}}\right) |\mathrm{H},\mathrm{H}\rangle\langle \mathrm{H},\mathrm{H}| - \frac{1}{\sqrt{3}} \mathrm{e}^{\mathrm{i}\phi} \sqrt{\delta R_{\mathrm{V}} \left(\frac{2}{3} - \delta R_{\mathrm{H}}\right)} (|\mathrm{V},\mathrm{H}\rangle\langle \mathrm{H},\mathrm{V}| + |\mathrm{H},\mathrm{V}\rangle\langle \mathrm{V},\mathrm{H}|) - \frac{1}{3} \mathrm{e}^{\mathrm{i}2\phi} \delta R_{\mathrm{V}}\, |\mathrm{V},\mathrm{V}\rangle\langle \mathrm{V},\mathrm{V}|\,. \tag{18}$$

In the case of perfect mode matching ($\xi = 1$), two-photon reflection and two-photon transmission are indistinguishable and the amplitudes of the output states interfere. Taking into account the correct phase relation given by the field operators, the effects of this quantum coherent operation on the two-photon polarization state are then given by

$$\hat{S}_{\mathrm{QC}} = \hat{S}_{\mathrm{R}} + \hat{S}_{\mathrm{T}}. \tag{19}$$

In the general case described by equations (13) and (14), the coherent operation has an amplitude of $\sqrt{\xi}$ and the mismatched output components have an amplitude of $\sqrt{1-\xi}$ each. After tracing out the ancillary degrees of freedom, this results in a statistical mixture of the coherent operation $\hat{S}_{\mathrm{QC}}$ with a statistical weight of $\xi = 1 - \delta\xi$ and the mismatched components $\hat{S}_{\mathrm{R}}$ and $\hat{S}_{\mathrm{T}}$ with a statistical weight of $1 - \xi = \delta\xi$. The process can then be represented by $\hat{\rho}_{\mathrm{out}} = E(\hat{\rho}_{\mathrm{in}})$ [23] with

$$E(\hat{\rho}) = (1 - \delta\xi)\hat{S}_{\mathrm{QC}}\hat{\rho}\hat{S}_{\mathrm{QC}}^{\dagger} + \delta\xi(\hat{S}_{\mathrm{R}}\hat{\rho}\hat{S}_{\mathrm{R}}^{\dagger} + \hat{S}_{\mathrm{T}}\hat{\rho}\hat{S}_{\mathrm{T}}^{\dagger}). \tag{20}$$

This equation was also used in the error analysis of Kiesel *et al* [15] for the estimation of a mode matching error in their experiment. The process E describes a linear map between the elements of the input density matrix and the elements of the output density matrix within the Hilbert space of two-photon polarization. This linear map can be expressed as a process matrix obtained by expanding the input density matrix and the output density matrix in terms of the operators $\{|i\rangle\langle j|\}$ associated with their matrix elements ρ_{ij}. Each column of the process matrix then corresponds to one of the 16 matrix elements of the input density matrix, and each line

corresponds to one of the 16 matrix elements of the output matrix. For example, the column of the process matrix for the input matrix element with $i = j = \mathrm{HH}$ is given by

$$E(|\mathrm{H,H}\rangle\langle\mathrm{H,H}|) = \left(\left(1-\frac{1}{2}\delta\xi\right)\left(\frac{1}{3}-2\delta R_{\mathrm{H}}\right)^{2}+\frac{1}{2}\delta\xi\right)|\mathrm{H,H}\rangle\langle\mathrm{H,H}|. \tag{21}$$

All the other 15 columns can be obtained in the same manner.

To compare the noisy process E with the quantum coherent operation $\hat{U}_{\mathrm{CZ}}$ given by equation (9), we use the process fidelity $F_{\mathrm{proc.}}$. In terms of the process matrix expansion given above, the process fidelity is [24]

$$F_{\mathrm{proc.}} = \frac{\sum_{i,j}\langle i|\,\hat{U}_{\mathrm{CZ}}^{\dagger}E(|i\rangle\langle j|)\,\hat{U}_{\mathrm{CZ}}\,|j\rangle}{\mathrm{Tr}\{\hat{U}_{\mathrm{CZ}}^{\dagger}\hat{U}_{\mathrm{CZ}}\}\mathrm{Tr}\{E(\hat{I})\}}, \tag{22}$$

where $\hat{I}$ is the identity operator in the four-dimensional Hilbert space of two photons each having two polarization degrees of freedom. Equations (20) and (22) define the process fidelity for any combination of experimental error sources. In the following, we will discuss the results for several interesting cases with the intention of defining the conditions for achieving fidelities close to one. We will therefore evaluate the effects of the errors in terms of the error rate ϵ, defined as the difference between the process fidelity and a perfect process fidelity of one,

$$\epsilon\,(\delta R_{\mathrm{H}}, \delta R_{\mathrm{V}}, \delta\phi, \delta\xi) = 1 - F_{\mathrm{proc.}}\,(\delta R_{\mathrm{H}}, \delta R_{\mathrm{V}}, \delta\phi, \delta\xi)\,. \tag{23}$$

Since the error rate is zero when all the errors are zero, the dependence of the error rate ϵ on the experimental error sources δR_{H}, δR_{V}, $\delta\phi$ and $\delta\xi$ is a direct measure of the impact of these errors on the performance of the linear optics quantum gate.

3. Results and discussion

In this section, we discuss the effect of error sources on the total error rate of the CZ gate. The error sources considered are the reflectance errors due to the deviations ($\delta R_{\mathrm{H}} = R'_{\mathrm{H}} - 1/3$ and $\delta R_{\mathrm{V}} = 1 - R'_{\mathrm{V}}$) of the actual reflectivities of PPBS-A (R'_{H}, R'_{V}) from the ideal ones ($R_{\mathrm{H}} = 1/3$, $R_{\mathrm{V}} = 1$), the birefringence error ($\delta\phi$) due to the phase difference (0 in the ideal case) between the horizontally polarized photons and the vertically polarized photons after passing through PPBS-A, and the mode mismatch error ($\delta\xi = 1 - \delta\xi'$) due to the spatio-temporal mode mismatch between the two input photons.

3.1. The reflectance error

The error rate ϵ for reflectance errors only ($\delta\phi = 0, \delta\xi = 0$) is shown in figures 4(A)–(C). Figure 4(A) shows the error rate as a function of δR_{H} with $\delta R_{\mathrm{V}} = 0$ (red solid curve) and $\delta R_{\mathrm{V}} = 0.015$ (blue dashed curve). For small δR_{H}, the dependence of ϵ on the reflectance errors is approximately quadratic. This means that the error ϵ due to δR_{H} rapidly diminishes for small δR_{H}. Note that the precise dependences of ϵ on δR_{H} are asymmetric to the vertical line $\delta R_{\mathrm{H}} = 0$; this is discussed in detail below. Figure 4(B) shows plots of ϵ as a function of δR_{V} with $\delta R_{\mathrm{H}} = 0$ and ± 0.04. The red solid line is for $\delta R_{\mathrm{H}} = 0$, while the blue dashed and black dotted lines are for $\delta R_{\mathrm{H}} = -0.04$ and $\delta R_{\mathrm{H}} = 0.04$, respectively. ϵ shows a linear dependence on δR_{V}. This is in contrast to the quadratic dependence on δR_{H}. As shown in figure 4(B), $\epsilon(\delta R_{\mathrm{H}} = 0.04)$ and $\epsilon(\delta R_{\mathrm{H}} = -0.04)$ are almost the same for $\delta R_{\mathrm{V}} = 0$ ($\epsilon = 0.015$). However, the two error rates

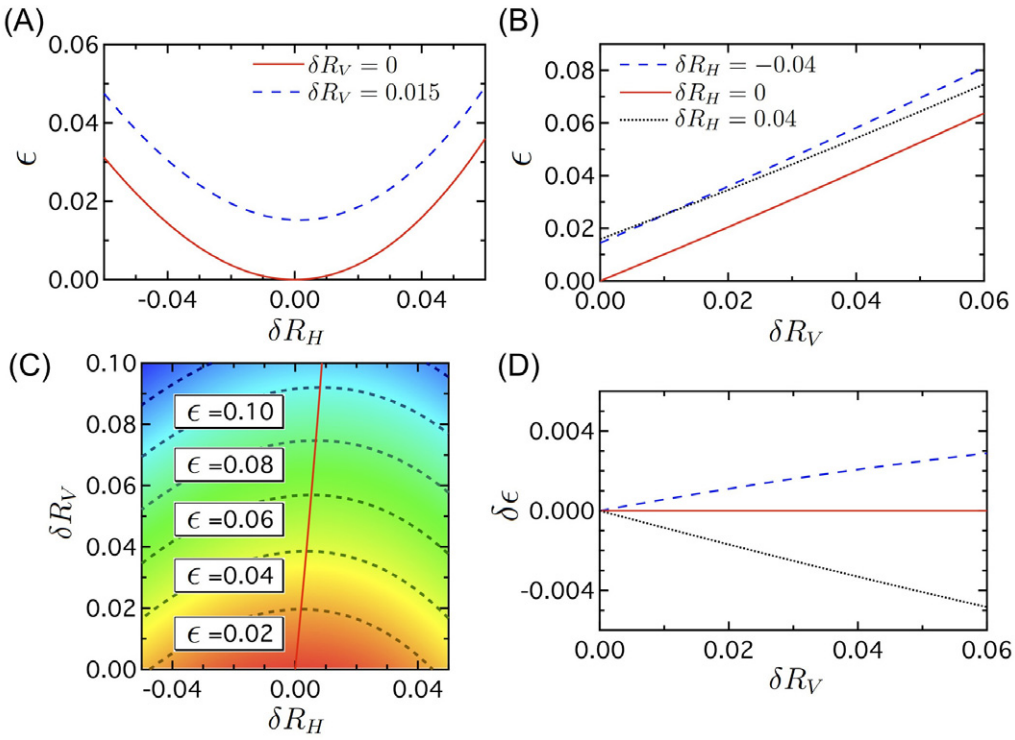

Figure 4. The errors caused by the reflectivities of PPBS-A. (A) Errors caused by δR_{H} in the case of $\delta R_{\mathrm{V}} = 0$ (red solid line) and $\delta R_{\mathrm{V}} = 0.015$ (blue dashed line). (B) Errors caused by δR_{V} in the case of $\delta R_{\mathrm{H}} = 0$ (red solid line), $\delta R_{\mathrm{H}} = -0.04$ (blue dashed line) and $\delta R_{\mathrm{H}} = 0.04$ (black dotted line). (C) Contour plot of ϵ as a function of δR_{H} and δR_{V}. (D) $\delta\epsilon$ as a function of δR_{V} when $\delta R_{\mathrm{H}} = 0$ (red solid line), $\delta R_{\mathrm{H}} = -0.04$ (blue dashed line), and $\delta R_{\mathrm{H}} = 0.04$ (black dotted line).

diverge as δR_{V} increases. This indicates that the errors due to δR_{H} and δR_{V} interact with each other.

To analyze this interaction of the error sources, figure 4(C) shows a contour plot of ϵ. The horizontal axis represents δR_{H} and the vertical axis represents δR_{V}. The red solid line indicates the optimum value of δR_{H} that minimizes ϵ for a certain value of δR_{V}. The line leans to the right, showing that errors in R_{H} can partially compensate for errors in R_{V}. This is a significant practical difference from the predictions of a linear error model, where errors can only add up.

To evaluate the interaction between different error sources, we define the deviation from the linear error model $\delta\epsilon$ as

$$\delta\epsilon\left(\delta A, \delta B\right) = \epsilon\left(\delta A, \delta B\right) - \left(\epsilon\left(\delta A, 0\right) + \epsilon\left(0, \delta B\right)\right), \tag{24}$$

where $\delta A, \delta B \in \{\delta R_{\mathrm{H}}, \delta R_{\mathrm{V}}, \delta\phi, \delta\xi\}$. $\delta\epsilon(\delta R_{\mathrm{H}}, \delta R_{\mathrm{V}})$ is plotted in figure 4(D) as a function of δR_{V}. By definition, $\delta\epsilon$ becomes 0 when $\delta R_{\mathrm{H}} = 0$ (red solid line). On the other hand, $\delta R_{\mathrm{H}} = -0.04$ (blue dashed line) and $\delta R_{\mathrm{H}} = 0.04$ (black dotted line) show an increase and a decrease in the error predicted by the linear error model, indicating that a positive error in R_{H} reduces the effect of the error in R_{V}, while a negative error increases it.

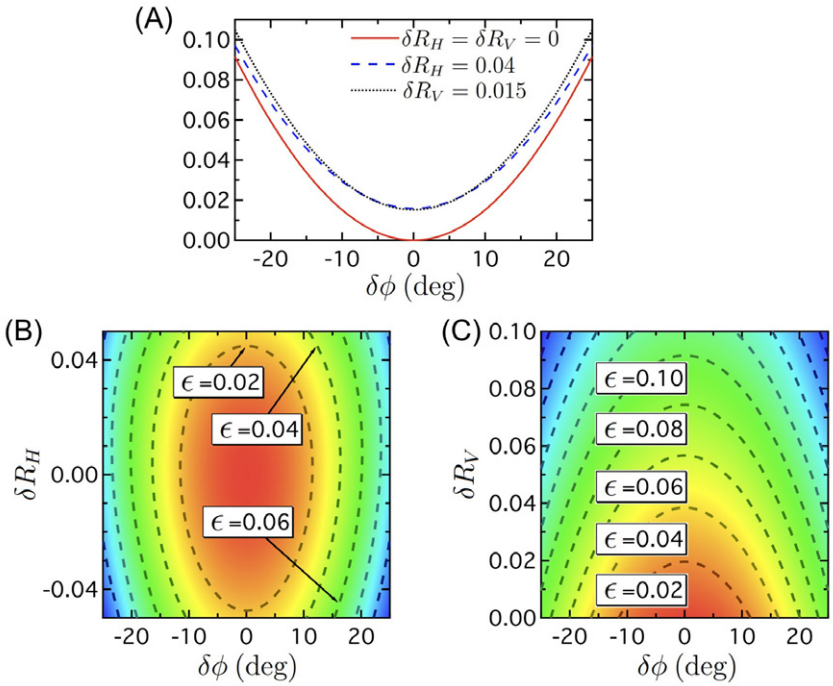

Figure 5. The errors caused by a birefringence error. (A) ϵ as a function of $\delta\phi$ for $\delta R_{\mathrm{H}} = 0$ and $\delta R_{\mathrm{V}} = 0$ (red solid curve), $\delta R_{\mathrm{H}} = 0.04$ and $\delta R_{\mathrm{V}} = 0$ (blue dashed curve), $\delta R_{\mathrm{H}} = 0$ and $\delta R_{\mathrm{V}} = 0.015$ (black dotted curve). Contour plots of ϵ for $\delta\phi$ against (B) δR_{H} and (C) δR_{V}.

3.2. The birefringence error

Figure 5 shows the error rate ϵ caused by a birefringence error. Figure 5(A) shows ϵ as a function of $\delta\phi$. The red solid line shows the result for $\delta R_{\mathrm{H}} = \delta R_{\mathrm{V}} = 0$, while the blue dashed line shows the result for $\delta R_{\mathrm{H}} = 0.04$ and $\delta R_{\mathrm{V}} = 0$, and the black dotted line shows the result for $\delta R_{\mathrm{H}} = 0$ and $\delta R_{\mathrm{V}} = 0.015$. The two values of δR_{H} and δR_{V} have been chosen to obtain an error rate of about $\epsilon = 0.015$ at $\delta\phi = 0$. Again, the dependence of ϵ on $\delta\phi$ is almost quadratic in all three cases, indicating that the effects of the birefringence error decrease rapidly as the error gets smaller. Note that, in the absence of other errors, the effect of the birefringence error ($\delta\phi$) can be given in a particularly simple analytical form, by substituting $\delta R_{\mathrm{H}} = \delta R_{\mathrm{V}} = \delta\xi = 0$ into equation (23):

$$\epsilon = 1 - \frac{(1+\cos\phi)^2}{4}. \tag{25}$$

Figures 5(B) and (C) show contour plots of ϵ for combinations of $\delta\phi$ with δR_{H} and δR_{V}, respectively. In both cases, ϵ is symmetric about a vertical line at $\phi = 0$. However, figure 5(B) shows a slight asymmetry with respect to the horizontal line at $\delta R_{\mathrm{H}} = 0$. As in figure 4(C), the value of δR_{H} that minimizes ϵ for a certain value of $\delta\phi$ is not zero. This indicates that the errors of R_{H} and ϕ can partially compensate each other, just like the errors of R_{H} and R_{V}. On the other hand, figure 5(C) does not show this kind of dependence. For any given $\delta\phi$, ϵ is always minimized at $\delta R_{\mathrm{V}} = 0$. However, this does not imply that these two factors are completely independent, since symmetric deviations from the linear error model are still possible.

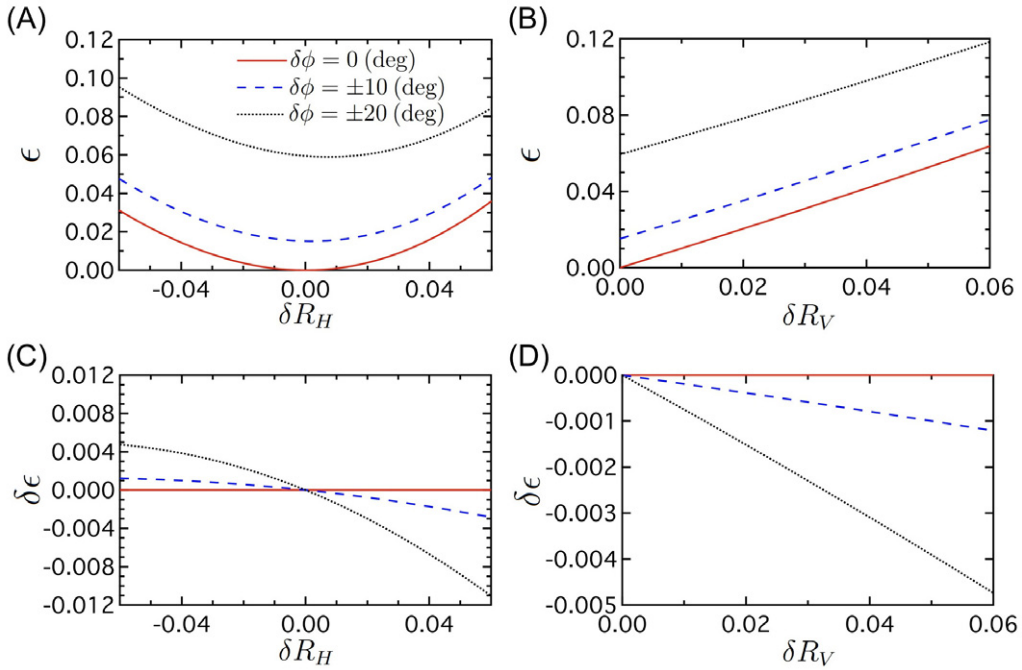

Figure 6. ϵ ($\delta\epsilon$) as a function of δR_{H} (A) ((C)) and as a function of δR_{V} (B) ((D)). The red solid lines show the case when $\delta\phi = 0$ (deg), while the blue dashed lines show $\delta\phi = 10$ (deg) and the black dotted lines show $\delta\phi = 20$ (deg).

To discuss the degree to which the birefringence error and the reflectance errors are independent of each other, we show the values of ϵ and $\delta\epsilon$ for various conditions in figure 6. Figures 6(A) and (C) show ϵ and $\delta\epsilon$ as functions of δR_{H} and figures 6(B) and (D) show ϵ and $\delta\epsilon$ as functions of δR_{V}. The graphs show the cases when $\delta\phi = 0$ (deg) (red solid line), $\delta\phi = \pm 10$ (deg) (blue dashed line) and $\delta\phi = \pm 20$ (deg) (black dotted line). ϵ increases quadratically with δR_{H}, while it increases linearly with δR_{V}. Figure 6(A) shows that ϵ is asymmetric with respect to δR_{H}, similar to figure 4(A). In figure 6(C), this asymmetry results in compensation of errors (negative $\delta\epsilon$) for positive δR_{H}, while the errors increase (positive $\delta\epsilon$) for negative δR_{H}. At $\delta R_{\mathrm{H}} = 0.04$ and $\delta\phi = 20$ (deg), $\delta\epsilon$ is -0.0067, which is 9.7% of the total error at this point ($\epsilon = 0.0686$). Thus, almost 10% of the error is compensated by the interaction between the two error sources. In contrast, $\delta\epsilon$ between δR_{V} and $\delta\phi$ is relatively small. At $\delta R_{\mathrm{V}} = 0.015$ and $\delta\phi = 20$ (deg), $\delta\epsilon$ is -0.0011, which is only 1.5% of the total error ($\epsilon = 0.0735$). Note that the comparison of these two cases is motivated by the fact that these combinations of δR_{H} and δR_{V} with $\delta\phi = 20$ (deg) have almost the same value of ϵ in the linear error model.

3.3. The mode mismatch error

Figure 7 shows a plot of ϵ as a function of $\delta\xi$. Figure 7(A) shows the region $0 < \delta\xi < 1$ and figure 7(B) shows the region $0 < \delta\xi < 0.2$. These plots are calculated assuming that there are no device errors ($\delta R_{\mathrm{H}} = 0$, $\delta R_{\mathrm{V}} = 0$, $\delta\phi = 0$). In the region where $\delta\xi$ is sufficiently small, ϵ is almost linear in $\delta\xi$. This means that the mode mismatch error remains a significant source of error even if $\delta\xi$ is very small. In the region shown in figure 7(B), an increase of $\delta\xi$ by about

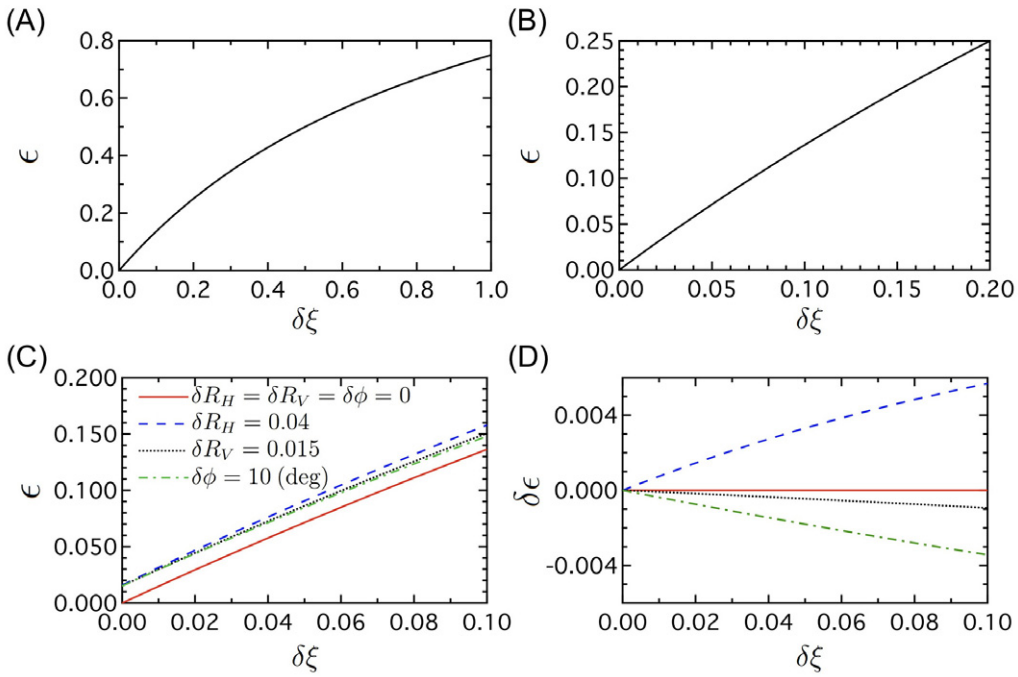

Figure 7. The error caused by the mode mismatch error. (A) $0 < \delta\xi < 1$. (B) $0 < \delta\xi < 0.2$. ((C) and (D)) Plots of ϵ and $\delta\epsilon$, respectively, as functions of $\delta\xi$ for $\delta R_{\mathrm{H}} = 0.04$ (red solid curve), $\delta R_{\mathrm{V}} = 0.015$ (blue dashed curve) and $\delta\phi = 10$ (deg) (green dash-dotted curve).

0.01 causes an increase of ϵ by about 0.013. Figure 7(D) shows the dependence of error rate on the mode mismatch error $\delta\xi$ in the presence of other device errors and figure 7(C) shows the error rate. The solid (dashed) line shows the case when $\delta R_{\mathrm{H}} = 0.04$ ($\delta R_{\mathrm{V}} = 0.015$) and the dash-dotted line shows the case when $\delta\phi = \pm 10$ (deg). All of these cases have almost the same error rate ($\epsilon = 0.015$) at $\delta\xi = 0$. For a positive error of $\delta R_{\mathrm{H}} = 0.04$, the effects of the mode matching errors are increased. On the other hand, an error of $\delta R_{\mathrm{V}} = 0.015$ results in a reduction of the effects of mode matching errors. However, this reduction is about six times smaller than the increase caused by the error in R_{H}. A more effective compensation of mode matching errors is achieved by the birefringence error, indicating the possibility of reducing the errors in two-photon interference by a simple phase shift in the single-photon outputs.

3.4. Conditions for a low-error gate

In this section, we consider the quality of the PPBS-A and the mode matching required for high-fidelity low-error gates. We estimated the values of parameters required to suppress ϵ to under 0.05, 0.01 and 0.001 for several conditions (table 1). About the error probability per gate for scalable quantum computation, 10^{-4} has been often quoted but 10^{-3} was suggested recently by Knill [20]. Unfortunately, the gate we analyzed is probabilistic (1/9) even when we assume the QND photon number detector in the output modes. Thus the 10^{-3} error threshold cannot be applicable to our case directly. However, we think that the analysis of error parameters for this threshold is informative.

Table 1. Conditions for achieving a high-fidelity gate when $\epsilon = 0.05$, 0.01 and 0.001. (i) Only one error source exists and the other parameters are ideal. (ii) Mode matching condition for a PPBS-A tested in our laboratory ($\delta R_H = 0.022$, $\delta R_V = 0.020$ and $\delta\phi = 3.5$ (deg)). (iii) Equal contributions to the error from all error sources.

	Condition (i)				Condition (ii)	Condition (iii)			
Parameter	δR_H	δR_V	$\delta\phi$	$\delta\xi$	$\delta\xi$	δR_H	δR_V	$\delta\phi$	$\delta\xi$
$\epsilon = 0.05$	0.071	0.0476	18.3	0.0345	0.0159	0.0363	0.0088	9.28	0.0129
$\epsilon = 0.01$	0.032	0.0100	8.1	0.0067	–	0.0161	0.0017	4.08	0.0025
$\epsilon = 0.001$	0.010	0.0010	2.6	0.00067	–	0.0051	0.00017	1.28	0.00025

Firstly, we evaluated the cases where only one error source exists and the other parameters are ideal. δR_H has positive and negative values, but here we show only the positive ones ($\delta R_H > 0$). To satisfy $\epsilon = 0.001$, δR_V must be ten times smaller than δR_H. At $\epsilon = 0.05$, the ratio is only about 1.5. This difference illustrates the difference between the quadratic dependence of ϵ on δR_H and the linear dependence of ϵ on δR_H. Likewise, the condition for mode matching becomes very severe at low errors. Table 1 thus shows that, for small errors, the most significant error sources are δR_V and $\delta\xi$.

Condition (ii) shows the mode matching requirement for an actual PPBS-A tested in our laboratory. The properties of this PPBS-A were $\delta R_H = 0.022$, $\delta R_V = 0.020$ and $\delta\phi = 3.5$ (deg). The PPBS-A is a cubic beam splitter made of an optical glass prism (BK7) with a specially designed dielectric multi-layer coating. This PPBS-A was designed to reduce the birefringence error; a conventional PPBS is therefore likely to have an even larger value of $\delta\phi$. As indicated in the table, we cannot suppress ϵ to 0.01 or below in this case, because the value of $\delta R_V = 0.020$ is larger than the limit of 0.010 required to achieve such error rates.

Finally, we calculated the case when the errors from all parameters are equal (condition (iii)). We searched for values of the parameters (δR_H, δR_V, $\delta\phi$, $\delta\xi$) that satisfy $\epsilon(\delta R_H) = \epsilon(\delta R_V) = \epsilon(\delta\phi) = \epsilon(\delta\xi)$ and $\epsilon(\delta R_H, \delta R_V, \delta\phi, \delta\xi) = 0.05$ or 0.01, or 0.001. As a result, the errors shown in table 1 decrease linearly with the error requirement for δR_V and $\delta\xi$, while the corresponding errors of δR_H and $\delta\phi$ decrease only with the square root. Again, the result shows that δR_V and $\delta\xi$ are the main sources of error for low-error gates.

4. Conclusions

We analyzed the errors in a linear-optics CZ gate caused by combinations of imperfect reflectivities and birefringence in the main optical component and a mode mismatch error between the separate input photons. We found that error rate depends linearly on the reflectivity error δR_V for the vertically polarized photons and the mode matching error $\delta\xi$, while its dependence on the reflectivity error δR_H for the horizontally polarized photons and the birefringence error $\delta\phi$ is only quadratic. We also evaluated the interaction between the error sources. In particular, we found that the effect of δR_H is strongly correlated with the effects of $\delta\phi$ and $\delta\xi$. In the case of a phase error of 20 degrees shown in figure 6, the deviation from the linear error model was found to be around 10% of the total error, indicating that the deviation from the linear error model can be quite significant under certain conditions.

The requirements for achieving high-fidelity gates were investigated for some specific cases, illustrating the significance of limiting the errors given by δR_{V} and $\delta\xi$ for the construction of low-error gates. Even though high-reflectivity mirrors with the sum of the transmittance and the loss ($\sim 1-R$) less than 10^{-5} has been realized [25], accurate control of the reflectivity and the phase may need future technical development. For minimizing spatial mode mismatch, gates in fibers [26] or waveguides [27] would be a suitable solution. Single-photon sources with small temporal jitter [28] are very important to minimize temporal mode mismatch. The analysis in this paper can easily be adapted to other linear optics quantum gates and may thus provide the foundation for a better understanding of experimental errors in a wide range of optical quantum information circuits. The cause of the different behavior of errors for the gate fidelity will be an interesting study.

Acknowledgments

This study was partially supported by a Grant-in-Aid for JSPS Fellows from the Japan Society for the Promotion of Science, a Grant-in-Aid for the Global COE Program from the Ministry of Education, Culture, Sports, Science and Technology, Core Research for Evolutional Science and Technology, Japan Science and Technology Agency and the Ministry of Internal Affairs and Communication, a Grant-in-Aid from the Japan Society for the Promotion of Science, Ministry of Internal Affairs and Communication and a Grant-in-Aid 'Quantum cybernetics' from the Japan Ministry of Education and Science, Promotion Society and the Special Coordination Funds for Promoting Science and Technology.

Appendix. Relationship between ξ and visibility V

We first consider the situation when horizontally polarized single photons are simultaneously input into a 50/50 non-polarizing beam splitter with both input modes. The output state from the beam splitter is then derived from equations (1), (13) and (14) with $R_{\mathrm{H}} = 1/2$,

$$
\begin{aligned}
|1,1\rangle_{\mathrm{a_{H0},b_H}} &= \hat{a}^{\dagger}_{\mathrm{H0}}\hat{b}^{\dagger}_{\mathrm{H}}\,|0\rangle \\
&= (\sqrt{\xi}\,\hat{a}_{\mathrm{H}} + \sqrt{1-\xi}\,\hat{a}_{\mathrm{H1}})^{\dagger}\hat{b}^{\dagger}_{\mathrm{H}}\,|0\rangle \\
&= \left(\sqrt{\xi}\,\frac{\hat{a}'_{\mathrm{H}} + \mathrm{i}\hat{b}'_{\mathrm{H}}}{\sqrt{2}} + \sqrt{1-\xi}\,\frac{\hat{a}'_{\mathrm{H1}} + \mathrm{i}\hat{b}'_{\mathrm{H1}}}{\sqrt{2}}\right)^{\dagger}\frac{(\mathrm{i}\hat{a}'_{\mathrm{H}} + \hat{b}'_{\mathrm{H}})^{\dagger}}{\sqrt{2}}\,|0\rangle \\
&= \frac{\sqrt{\xi}}{2}(\mathrm{i}\hat{a}'^{2}_{\mathrm{H}} + \mathrm{i}\hat{b}'^{2}_{\mathrm{H}})^{\dagger}\,|0\rangle \\
&\quad + \frac{\sqrt{1-\xi}}{2}(\mathrm{i}\hat{a}'_{\mathrm{H}}\hat{a}'_{\mathrm{H1}} + \mathrm{i}\hat{b}'_{\mathrm{H1}}\hat{b}'_{\mathrm{H}} + \hat{a}'_{\mathrm{H1}}\hat{b}'_{\mathrm{H}} - \hat{a}'_{\mathrm{H}}\hat{b}'_{\mathrm{H1}})^{\dagger}\,|0\rangle \\
&= -\mathrm{i}\frac{\sqrt{\xi}}{\sqrt{2}}\left(|2\mathrm{H},0\rangle_{\mathrm{a'},\mathrm{b'}} + |0,2\mathrm{H}\rangle_{\mathrm{a'},\mathrm{b'}}\right) \\
&\quad + \frac{\sqrt{1-\xi}}{2}(-\mathrm{i}\,|\mathrm{H},0\rangle_{\mathrm{a'},\mathrm{b'}} \otimes |\mathrm{H},0\rangle_{\mathrm{a1'},\mathrm{b1'}} - \mathrm{i}\,|0,\mathrm{H}\rangle_{\mathrm{a'},\mathrm{b'}} \otimes |0,\mathrm{H}\rangle_{\mathrm{a1'},\mathrm{b1'}}) \\
&\quad + \frac{\sqrt{1-\xi}}{2}(|\,0,\mathrm{H}\rangle_{\mathrm{a'},\mathrm{b'}} \otimes |\mathrm{H},0\rangle_{\mathrm{a1'},\mathrm{b1'}} - |\mathrm{H},0\rangle_{\mathrm{a'},\mathrm{b'}} \otimes |0,\mathrm{H}\rangle_{\mathrm{a1'},\mathrm{b1'}}).
\end{aligned}
\tag{A.1}
$$

Therefore, the probability of coincidence detection at both outputs is

$$P_Q = \frac{1-\xi}{2}. \tag{A.2}$$

On the other hand, the coincidence detection probability when two photons arrive at the beam splitter with a sufficiently large time difference is $P_{NQ} = 1/2$. Therefore, the visibility of the Hong–Ou–Mandel interference in this case is

$$V = \frac{P_{NQ} - P_Q}{P_{NQ}} = \xi. \tag{A.3}$$

References

[1] Gisin N, Ribordy G G, Tittel W and Zbinden H 2002 Quantum cryptography *Rev. Mod. Phys.* **74** 145–95

[2] Nagata T, Okamoto R, O'Brien J L, Sasaki K and Takeuchi S 2007 Beating the standard quantum limit with four-entangled photons *Science* **316** 726–9

[3] Higgins B L, Berry D W, Bartlett S D, Wiseman H M and Pryde G J 2007 Entanglement-free Heisenberg-limited phase estimation *Nature* **450** 393–6

[4] Boto A N, Kok P, Abrams D S, Braunstein S L, Williams C P and Dowling J P 2000 Quantum interferometric optical lithography: exploiting entanglement to beat the diffraction limit *Phys. Rev. Lett.* **85** 2733–6

[5] Kawabe Y, Fujiwara H, Okamoto R, Sasaki K and Takeuchi S 2007 Quantum interference fringes beating the diffraction limit *Opt. Express* **15** 14244–50

[6] Chuang I L and Yamamoto Y 1995 Simple quantum computer *Phys. Rev.* A **52** 3489

[7] Knill E, Laflamme R and Milburn G J 2001 A scheme for efficient quantum computation with linear optics *Nature* **409** 46–52

[8] Takeuchi S, Kim J, Yamamoto Y and Hogue H H 1999 Development of a high-quantum-efficiency single-photon counting system *Appl. Phys. Lett.* **74** 1063–5

[9] Kim J S, Takeuchi S, Yamamoto Y and Hogue H H 1999 Multiphoton detection using visible light photon counter *Appl. Phys. Lett.* **74** 902–4

[10] Strauf S, Stoltz N G, Rakher M T, Coldren L A, Petroff P M and Bouwmeester D 2007 High-frequency single-photon source with polarization control *Nat. Photonics* **1** 704–8

[11] Hofmann H F and Takeuchi S 2002 Quantum phase gate for photonic qubits using only beam splitters and postselection *Phys. Rev.* A **66** 024308

[12] Ralph T C, Langford N K, Bell T B and White A G 2002 Linear optical controlled-NOT gate in the coincidence basis *Phys. Rev.* A **65** 062324

[13] Okamoto R, Hofmann H F, Takeuchi S and Sasaki K 2005 Demonstration of an optical quantum controlled-NOT gate without path interference *Phys. Rev. Lett.* **95** 210506

[14] Langford N K, Weinhold T J, Prevedel R, Resch K J, Gilchrist A, O'Brien J L, Pryde G J and White A G 2005 Demonstration of a simple entangling optical gate and its use in Bell-state analysis *Phys. Rev. Lett.* **95** 210504

[15] Kiesel N, Schmid C, Weber U, Ursin R and Weinfurter H 2005 Linear optics controlled-phase gate made simple *Phys. Rev. Lett.* **95** 210505

[16] Okamoto R, O'Brien J L, Hofmann H F, Nagata T, Sasaki K and Takeuchi S 2009 An entanglement filter *Science* **323** 483–5

[17] Lanyon B P, Weinhold T J, Langford N K, Barbieri M, James D F V, Gilchrist A and White A G 2007 Experimental demonstration of a compiled version of Shor's algorithm with quantum entanglement *Phys. Rev. Lett.* **99** 250505

[18] Lanyon B P, Barbieri M, Almeida M P, Jennewein T, Ralph T C, Resch K J, Pryde G J, O'Brien J L, Gilchrist A and White A G 2009 Simplifying quantum logic using higher-dimensional Hilbert spaces *Nat. Phys.* **5** 134–40

[19] Weinhold T J, Gilchrist A, Resch K J, Doherty A C, O'Brien J L, Pryde G J and White A G 2008 Understanding photonic quantum-logic gates: the road to fault tolerance arXiv:0808.0794
[20] Knill E 2005 Quantum computing with realistically noisy devices *Nature* **434** 39–44
[21] Hong C K, Ou Z Y and Mandel L 1987 Measurement of subpicosecond time intervals between 2 photons by interference *Phys. Rev. Lett.* **59** 2044–6
[22] Campos R A, Saleh B E A and Teich M C 1989 Quantum-mechanical lossless beam splitter—SU(2) symmetry and photon statistics *Phys. Rev.* A **40** 1371–84
[23] Nielsen M A and Chuang I L 2000 *Quantum Computation and Quantum Information* (Cambridge: Cambridge University Press)
[24] Hofmann H F, Okamoto R and Takeuchi 2006 Analysis of an experimental quantum logic gate by complementary classical operations *Mod. Phys. Lett.* A **21** 1837–50
[25] Hood C J, Kimble H J and Ye J 2001 Characterization of high-finesse mirrors: loss, phase shifts, and mode structure in an optical cavity *Phys. Rev.* A **64** 033804
[26] Clark A S, Fulconis J, Rarity J G, Wadsworth W J and O'Brien J L 2009 All-optical-fiber polarization-based quantum logic gate *Phys. Rev.* A **79** 030303
[27] Politi A, Cryan M J, Rarity J G, Yu S and O'Brien J L 2009 Silica-on-silicon waveguide quantum circuits *Science* **320** 646–9
[28] Tanida M *et al* in preparation